

## NEW SEISMICITY BASED SEISMIC SOURCES AND HAZARD MODEL FOR PERU

Z. Aguilar<sup>1</sup> & J. Tarazona<sup>2</sup>

<sup>1</sup> National University of Engineering, Lima, Peru, zaguilar@uni.edu.pe

<sup>2</sup> National University of Engineering, Lima, Peru

**Abstract:** In seismic design, intensity parameters are used to represent the seismic demand; however, in regions with limited information, the selection of these parameters may be controversial. Likewise, a probabilistic seismic hazard assessment is used to evaluate this demand. In Peru, the selection of seismogenic sources and their maximum seismic magnitudes to evaluate the regional seismic hazard has been a challenge due to the limited information available on significant events and subjective decisions in the zoning of seismic sources. In this study, a seismic zonation of Peru has been performed using several approaches based on seismicity and geology. The seismic catalog was updated to the year 2022, generating 34 seismic sources (7 interface, 15 intraplate and 12 crustal) with their corresponding maximum magnitudes. These maximum magnitudes are in the range of  $M_w$  8.7-9.0 for interface sources and  $M_w$  7.7-8.0 for intraplate sources. Furthermore, seismic hazard maps for return periods of 475 and 2475 years have been generated based on these models, from which it is possible to appreciate consistency in their boundaries with studies of neighboring countries, which represents a good step to follow in the updating of seismic design maps in Peru.

### 1. Introduction

The task of predicting how and when the ground will shake due to seismic events is critical to many areas of engineering and risk management. In this context, Probabilistic Seismic Hazard Analysis (PSHA) plays a fundamental role by providing a methodology for estimating measures of ground motion intensity based on the seismicity of a region.

To perform a proper PSHA, it is essential that the local seismicity and geologic characteristics of the region are accurately represented. This is typically accomplished by defining seismogenic sources, which delineate areas with similar seismic characteristics from seismicity and geology-based approaches. These approaches mainly provide us with the occurrence rates of seismic events and the maximum magnitude ( $M_{max}$ ) of each seismogenic source (Baker, Bradley and Stafford, 2021).

However, a challenge arises in locations where historical earthquake information is limited or incomplete. In such circumstances, it is not uncommon for the  $M_{max}$  values considered in the PSHA to exceed the historically observed values. Peru is a clear example of this situation. Although there are several seismotectonic model proposals (e.g. Tavera *et al.*, 2014; Roncal *et al.*, 2017), they often present  $M_{max}$  estimates that are inconsistent with recent seismic events, physical studies (e.g. Okal, Borrero and Synolakis, 2006; Pulido *et al.*, 2015), or historical seismic catalogs (Silgado, 1978; Dorbath, Cisternas and Dorbath C., 1990).

Against this background, the main objective of this study is to delimit the subduction seismic sources in Peru and to assess the seismic hazard in this country. For this purpose, the Peruvian seismic catalog has been updated and several approaches have been implemented, including the  $M_{\max}$  zonings performed by Tarazona *et al.* (2023), in addition to the seismic and geological characteristics described by Villegas-Lanza *et al.* (2016). This analysis has allowed a more reasonable characterization of the seismic sources, resulting in a proposal consistent with the interseismic moment deficit accumulation zones and rupture areas of large subduction earthquakes. As a result, the seismic recurrence values and finally, the probabilistic seismic hazard maps of Peru have been updated.

## 2. Seismic Catalogue

Seismic events were collected in a spatial window defined between the parallels 7°N and 28°S and the meridians 63°W and 86°W; and until the year 2022. The seismic catalog was compiled from events reported in nine seismic catalogs published by the Geophysical Institute of Peru (IGP), the International Seismological Center (ISC, ISC-REV and ISC-GEM), the Centroid Moment Tensor (CMT), the United States Geological Survey (USGS), the National Oceanic and Atmospheric Administration (NOAA), the South American Risk Assessment (SARA), and the Northern California Earthquake Data Center (NCEDC). Only seismic events with  $M_w \geq 4.0$  and historical events within the aforementioned spatiotemporal window were considered.

The magnitude scales were standardized to the  $M_w$  scale using the expressions proposed by Scordilis (2006). Likewise, the elimination of duplicates was performed based on the analysis of temporal and spatial variation between events, following the procedure described by Tarazona *et al.* (2023). Subsequently, events were categorized as interface, intraslab, crustal and unclassified according to the criteria established by Pagani, Johnson and Garcia Palaez (2020) using the USGS - Slab 2.0 subduction model (Hayes *et. al.*, 2018) and the LITHO 1.0 crustal model (Pasyanos *et al.*, 2014). A buffer zone of 10 km below the Moho discontinuity was used for crustal events, 20 km above and 100 km below Slab 2.0 for intraslab, and 35 km on either side of the Slab 2.0 for interface (Figure 1). Events not belonging to any of the above zones were labeled as "unclassified". Instrumental events with undefined or predetermined depths with  $M_w < 6.0$  were not included in the catalog, and historical events without depth were manually classified.

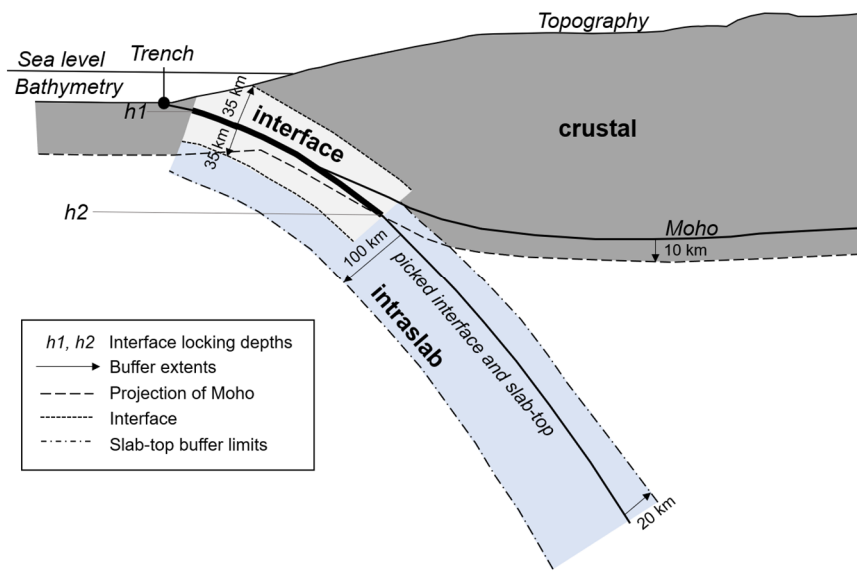


Figure 1. Classification of seismic mechanisms. Adapted from Pagani, Johnson, Garcia Palaez (2020).

After a manual review of the classification of the seismic mechanisms, aftershocks or precursors were eliminated using the methodology proposed by Gardner and Knopoff (1974) using the time windows proposed by Uhrhammer (1986).

A completeness analysis of each mechanism was then performed using the graphical method of Stepp (1972), and, the years of completeness for each magnitude range are shown in Table 1.

*Table 1. Completeness times by seismic mechanism*

Mw	Year of completeness		
	Interface	Intraslab	Crustal
4.5 - 5.4	1960	1960	1991
5.5 - 5.9	1960	1960	1960
6.0 - 6.9	1900	1900	1920
7.0 - 7.4	1900	1900	1616
>= 7.5	1513	1715	-

The results indicate that, in the compiled catalog for subduction earthquakes, information is available and complete since 1960 for  $4.5 \leq M_w < 6.0$  and since 1900 for  $6.0 \leq M_w < 7.5$ . In the case of seismic events with magnitudes equal to or greater than 7.5, we have applied a completeness period corresponding to the year in which the first seismic event in this range was recorded for each type of seismic mechanism: the  $M_w$  7.5 earthquake of 1715 for intraslab and  $M_w$  8.7 of 1513 for interface. Finally, for crustal earthquakes, shorter times of completeness were obtained than for subduction, and in the case of seismic events with magnitudes equal to or greater than 7.0, a time of completeness was considered from the year 1616, corresponding to an earthquake of  $M_w$  7.0.

Although the historical seismic catalog of Peru begins in the year 1471 with an event of  $M_S = 8.0$  (Tavera, 2001), this event was excluded from the catalog because of uncertainty in its magnitude and because it was associated with the eruption of the Misti volcano (Silgado, 1978).

### 3. Delimitation of Seismogenic Sources

#### 3.1. Interface sources

The interface subduction segments in Peru can be classified into three distinct zones. These zones have similar characteristics and seismic potential.

In the northern segment of Peru, north of the Mendaña fracture, the determination of the moment deficit has high uncertainty and a lack of historical records of large earthquake (Villegas-Lanza *et al.*, 2016; Nishenko, 1991).

The central segment is naturally bounded by the Mendaña fracture and the Nazca Ridge, with estimates suggesting the possibility of ruptures with a magnitude equal to or greater than  $M_w = 8.6$  (Pulido *et al.*, 2015, 2023).

In the southern segment, Villegas-Lanza *et al.* (2016) identified two areas of significant interseismic moment deficit accumulation. The one closest to the city of Tacna in southern Peru suggests a possible rupture scenario with a magnitude of  $M_w = 8.5$  (Pulido *et al.*, 2014). In contrast, Okal, Borrero and Synolakis (2006) argue that the rupture model derived from the 1868 Arica earthquake event, based on the calculations of Dorbath, Cisternas and Dorbath C. (1990), does not explain the level of destruction observed in the city of Pisco. This suggests that the Nazca Ridge could act as an obstacle for certain seismic events, but some earthquakes may not be limited by this geological feature in their rupture process.

With respect to the maximum magnitudes associated with each interface subduction segment, Tarazona *et al.* (2023) proposed a zonation of the maximum interface magnitudes based on a smoothed model of the maximum magnitude obtained using the Kijko (2004) method and the Bayesian approach (Johnston *et al.*, 1994; EPRI, U.S. DOE and U.S. NRC, 2012).

Since source delineations have a significant impact on the determination of occurrence rates, it was necessary to establish compatibility between the three types of approaches commonly used to perform this task (Baker, Bradley and Stafford, 2021): the seismicity-based approach, resulting from the incorporation of the  $M_{max}$  delineations proposed by Tarazona *et al.* (2023); the geological approach, from the inclusion of the geological barriers present in the region (Sparks *et al.*, 2010; Watts, Koppers and Robinson, 2010); and earthquake

simulation, from the available studies of the moment deficit present in each segment (Villegas-Lanza *et al.*, 2016; Pulido *et al.*, 2014, 2015, 2023).

As a result, Figure 2 shows the 4 main segments identified on the Peruvian coast. The first one corresponds to segment F-3a, with a shallow moment deficit, considered as a possible source in its entirety from the experience of shallow focus ruptures such as the 2011  $M_w=9.1$  Tohoku earthquake (Lay, 2018). The second segment, F-4a, with historical scenarios is located between the Mendaña fracture (MFZ) and the Nazca Ridge (NR). The third and fourth segments comprise the F-5a source, which includes two moment deficit accumulation zones, historically characterized by a rupture of both zones, possibly extending to the Nazca Ridge (Okal, Borrero and Synolakis, 2006).

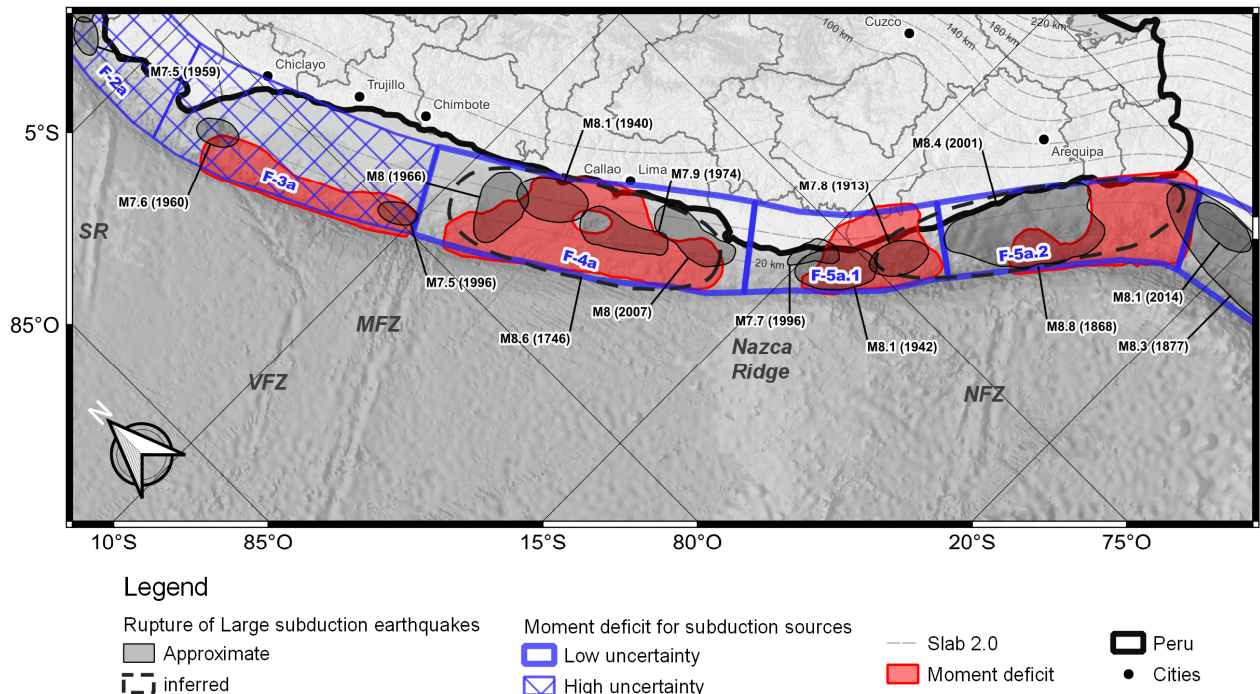


Figure 2. Delimitation of interface seismogenic sources on the Peruvian coast.

To determine the maximum magnitudes of the subduction sources, mainly two methods based on extreme value statistics were used to estimate the  $M_{max}$  ( $M_{max}^K$ ).

The method of Kijko (2004) uses a complete seismic catalog declustered above a threshold magnitude ( $M_0$ ) with a certain number of events ( $n$ ) and seismic recurrence ( $\beta$ ), where the  $M_{max}$  is calculated recursively from the maximum observed magnitude of  $M_{max}^{obs}$  and using Eqs. 1 and 2.

$$M_{max}^K = M_{max}^{obs} + \int_{M_0}^{M_{max}} F_{M_n}(m) dm = M_{max}^{obs} + \Delta \quad (1)$$

$$\Delta = \int_{M_0}^{M_{max}^K} \left[ \frac{1 - \exp [-\beta(m - M_0)]}{1 - \exp [-\beta(M_{max}^{obs} - M_0)]} \right]^n dm \quad (2)$$

In the equations shown, the value of  $\Delta$  is a function of  $\beta$ ,  $M_{max}$ ,  $M_0$  and  $n$ . Also, according to Kijko (2004), this method estimates  $M_{max}$  more accurately for values of  $n$  greater than 50 and 150 when the range of magnitudes ( $M_{max} - M_0$ ) is not greater than two and three degrees of magnitude, respectively.

On the other hand, the Bayesian approach (Johnston *et al.*, 1994) provides a more stable approximation than the method of Kijko (2004) in regions of low seismicity because the limited availability of data makes it difficult to estimate  $M_{max}^K$ . This is because the observed value of  $M_{max}^{obs}$  is generally lower than the probable value of  $M_{max}$  or a low value of  $n$ . First, the tectonic setting of the study region was classified and  $M_{max}^{obs}$  statistics from similar regions were collected to obtain a regional distribution function of  $M_{max}^{obs}$ . In the second step, the "a

"priori" distribution is obtained by modifying the regional distribution with the cumulative distribution function of the seismic recurrence and the number of earthquakes in the study area. Finally, the a priori distribution is updated using the likelihood function of Eq. 3, where  $\Delta_M = (M_{max} - M_0)$ , resulting in the expected distribution of  $M_{max}$  using the Bayesian approach  $M_{max}^B$ .

$$\mathcal{L}(M_{max}|m, \beta) = \begin{cases} 0, & m < M_{max}^{obs} \\ \left(\frac{1}{1 - \exp[-\beta\Delta_M]}\right)^n, & m \geq M_{max}^{obs} \end{cases} \quad (3)$$

To the previously described methods, we added the maximum magnitude estimates from the rupture scale relations for subduction earthquakes ( $M_{max}^{S-R}$ ) proposed by Allen and Hayes (2017) and the empirical approach consisting of adding an increment to the  $M_{max}^{obs}$  ( $M_{max}^A$ ) (Wheeler, 2009). For the latter approach, we considered an increment of 0.2 for sources with  $M_{max}^{obs}$  greater than or equal to  $M_w=8.5$ .

Table 2 summarizes the values obtained by all the above approaches and the recommended value of  $M_{max}$  for each interface source.

*Table 2. Estimation of  $M_{max}$  for interface sources*

Source	$M_{max}^{obs}$	$M_{max}^A$	$M_{max}^K$	$M_{max}^B$	$M_{max}^{S-R}$	$M_{max}$
F-1a	8.5	8.7	8.7	8.8	8.8	$8.8 \pm 0.1$
F-2a	7.8	*	8.7	8.7	8.8	$8.7 \pm 0.1$
F-3a	7.9	*	8.7	8.7	8.9	$8.8 \pm 0.1$
F-4a	8.6	8.8	8.9	8.7	9.0	$8.9 \pm 0.1$
F-5a	8.8	9.0	8.9	9.0	9.0	$9.0 \pm 0.1$
F-5a.1	7.8	*	**	**	8.5	$8.5 \pm 0.0$
F-5a.2	8.5*	8.7	**	**	8.5	$8.6 \pm 0.0$
F-6a	8.3	*	8.9	8.9	9.1	$9.0 \pm 0.1$

*Note:*

\* Not included in the analysis due to low observed seismicity.

\*\* Omitted because both sub-sources only separate areas of roughness from source F-5a.

### 3.2. Intraslab sources

For the delineation of the intraslab seismogenic source, the seismicity-based approach and the geological approach were mainly considered.

To estimate the maximum magnitude of these sources the same methods were used as for the interface sources. However, for the scaling relations proposed by Allen and Hayes (2017), a factor of 90% of the Slab 2.0 thickness of each source was used (Tarazona *et al.*, 2023), resulting in a reference value of ( $M_{max}^{S-R}$ ) . Likewise, a  $\Delta$  of 0.5 ° to  $M_{max}^{obs}$  was used to estimate ( $M_{max}^A$ ), but without exceeding a maximum value of  $M_w$  8.2, a value considered due to its proximity to the Calama earthquake in 1950 (United States Geological Survey, 2020).

Finally, because the Nazca slab in northern Peru subducts sub-horizontally between sources F-3b and F-3c, an additional source (F-3bc) encompassing the previous ones was also considered.

Table 3 lists the values obtained by all the above approaches and the recommended value of  $M_{max}$  obtained for each intraslab source.

Table 3. Estimation of  $M_{max}$  for intraslab sources

Fuente	$M_{max}^{obs}$	$M_{max}^{\Delta}$	$M_{max}^K$	$M_{max}^B$	$M_{max}^{S-R}$	$M_{max}$
F-1b.1	7.3	7.8	7.7	7.7	7.7	$7.7 \pm 0.0$
F-1b.2	7.6	8.1	7.7	7.9	7.8	$7.9 \pm 0.1$
F-1c	7.5	8.0	7.7	7.8	7.8	$7.8 \pm 0.1$
F-2b	7.1	7.6	7.7	7.7	7.9	$7.7 \pm 0.1$
F-2c	7.4	7.9	7.7	7.8	7.9	$7.8 \pm 0.1$
F-3bc	8.0	8.2	8.1	8.2	8.0	$8.0 \pm 0.1$
F-3b	7.9	8.2	8.1	8.0	8.0	$8.0 \pm 0.0$
F-3c	8.0	8.2	8.1	8.1	8.0	$8.0 \pm 0.1$
F-4b	7.7	8.2	7.8	7.9	8.2	$7.9 \pm 0.1$
F-4c.1	7.0	7.5	7.2	7.7	8.1	$7.7 \pm 0.2$
F-4c.2	7.6	8.1	7.7	7.9	8.2	$7.9 \pm 0.1$
F-5b.1	7.3	7.8	7.5	7.7	8.2	$7.7 \pm 0.2$
F-5c.1	7.4	7.9	7.6	7.8	8.2	$7.8 \pm 0.2$
F-5b.2	7.5	8.0	7.7	7.8	8.2	$7.8 \pm 0.2$
F-5c.2	7.6	8.1	7.8	7.8	8.2	$7.8 \pm 0.2$
F-6b	8.2	8.2	8.3	8.3	8.2	$8.2 \pm 0.0$

### 3.3. Crustal sources

The crustal sources have been modified from the proposal of Roncal (2017), according to the location with respect to the Peruvian western (PSw) and eastern (PSe) fringe, as delimited by the study of Villegas-Lanza *et al.* (2016). The main changes in this proposal include the splitting of source F-29 of Roncal (2017), the updating of the maximum magnitudes of all sources, and the addition of two crustal sources, at the border with Ecuador (PSw-1) and in the Peruvian jungle (PSe-4). The maximum magnitudes were obtained from the method of Kijko (2004), resulting in a maximum magnitude of up to  $M_w = 7.4$ . However, we consider that in future studies it will be necessary to incorporate a geological evaluation of the maximum magnitudes based on the analysis of the different fault systems present in the Peruvian continental zone.

Finally, the proposed seismogenic source model consists of 7 interface subduction sources, 15 intraslab subduction sources and 12 crustal sources, as shown in Figure 3.

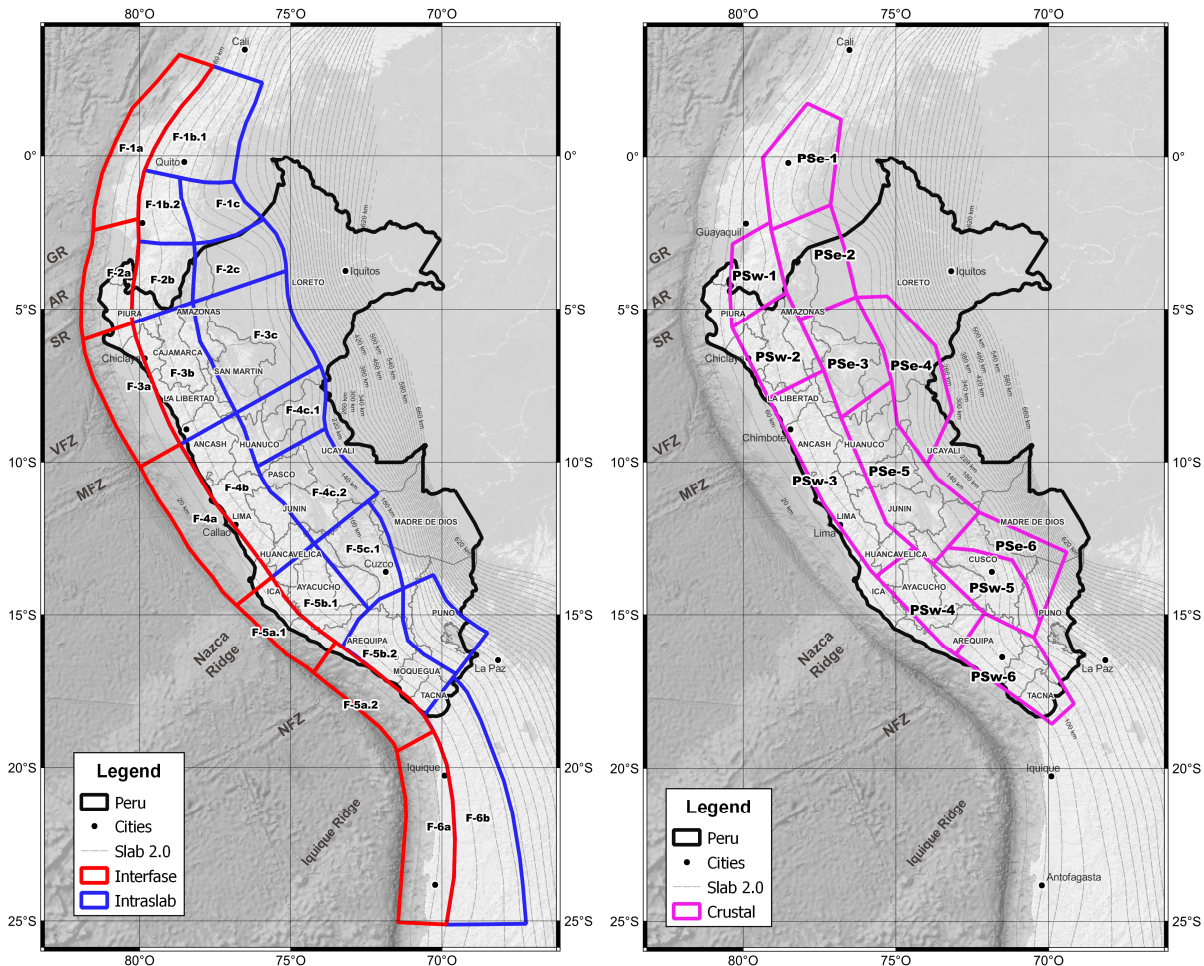


Figure 3. Peruvian Seismogenic sources

#### 4. Seismic Hazard Assessment

Seismic recurrence analysis was performed following the methodology of Weichert (1980), using a typical minimum magnitude ( $M_{\min}$ ) of  $M_w = 5.0$  (Bommer and Crowley, 2017) and an optimized curve fit of  $M_w 5.5$  or  $6.0$  to the  $M_{\max}$  of each source represented by a modified or exponentially truncated GR model (Baker, Bradley and Stafford, 2021), see Figure 4.

Following the recommendations of Strasser, Bommer and Abrahamson (2008), a truncation level of 3 was considered in the used ground motion models (GMMs), which were selected from the maximum likelihood (LLH) analysis (Scherbaum, Delavaud, and Riggelsen, 2009) of a database of Peruvian subduction earthquakes, considering only events with magnitudes equal to or greater than  $M_w 5.0$  and with rupture distances ( $R_{rup}$ ) less than 350 km with site classifications B and C, according to ASCE 7-16 (2017). However, since the largest recorded earthquake was the 2001 earthquake with a magnitude of  $M_w 8.4$ , an assessment of the maximum magnitude extrapolation of the interface GMMs was included (Figure 5). This assessment was performed from the synthetic accelerograms generated by the  $M_w 8$  events simulated by Pulido *et al.* (2015) for central Peru and, additionally, from the seismic records of the 2010 Chilean  $M_w=8.8$  earthquake (Bastías and Montalva, 2016); both for soil site classifications B and C.

The results obtained suggest that, in most cases, the observed subduction seismicity is compatible with the GMMs of Montalva, Bastías and Rodriguez-Marek (2017), Parker *et al.* (2020), Abrahamson and Gülerce (2020), Kuehn *et al.* (2020). Using the methodology described by Scherbaum, Delavaud and Riggelsen (2009), the weighting factors of these GMMs were obtained as shown in Table 4.

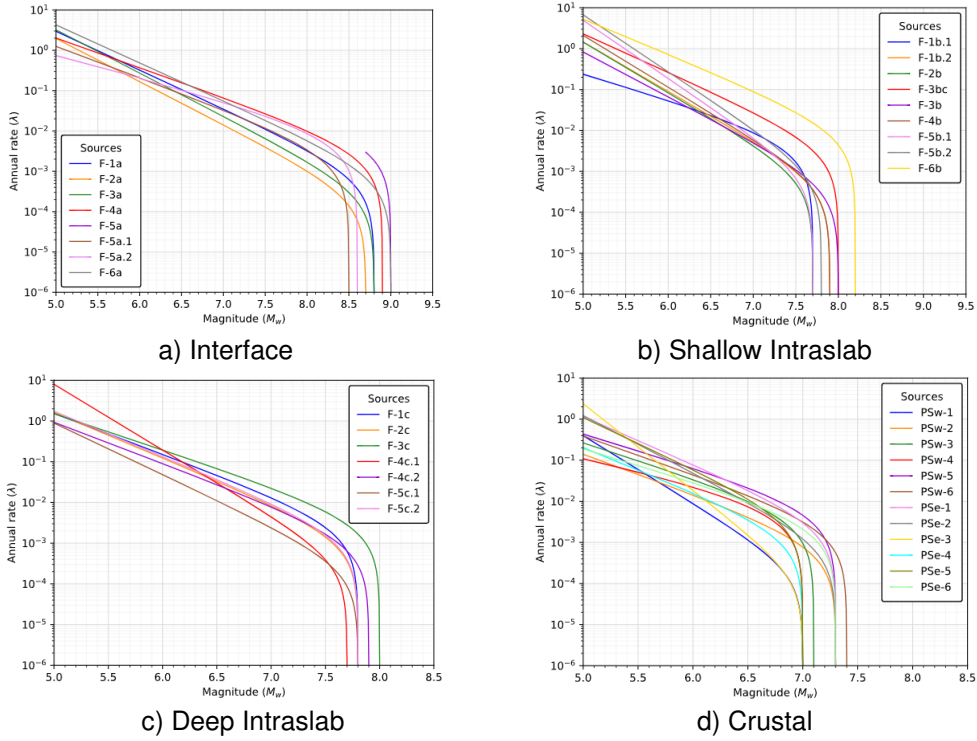


Figure 4. Seismic recurrence analysis

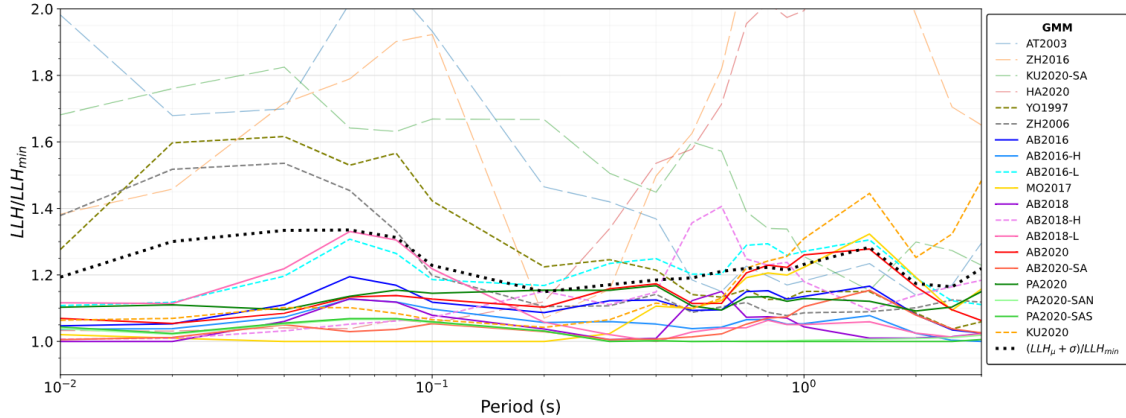


Figure 5. Normalised goodness-of-fit for interface earthquakes for large events.

Table 4. Weighting of GMMs

GMM	Code	Interface		Intraslab	
		Version*	Code	Version*	Weight
Abrahamson <i>et al.</i> (2020)	AB2020	SA	34%	Global, SA	25%
Parker <i>et al.</i> (2020)	PA2020	SAN, SAS	33%	Global, SAN, SAS	25%
Montalva <i>et al.</i> (2017)	MO2017	Global	33%	Global	25%
Kuehn <i>et al.</i> (2020)	KU2020	-	-	Global, SA	25%

Note:

\* Regionalizations of the models: Global, South America (SA), South America South and North (SAS and SAN).

Finally, the seismic hazard assessment by the probabilistic method was calculated using the software R-CRISIS v.20.2.0 (Ordaz *et al.*, 2017), based on the methodology proposed by Cornell (1968), for a representative  $V_{S30}$  of 760 m/s and for return periods (Tr) of 475 and 2475 years (Figure 6).

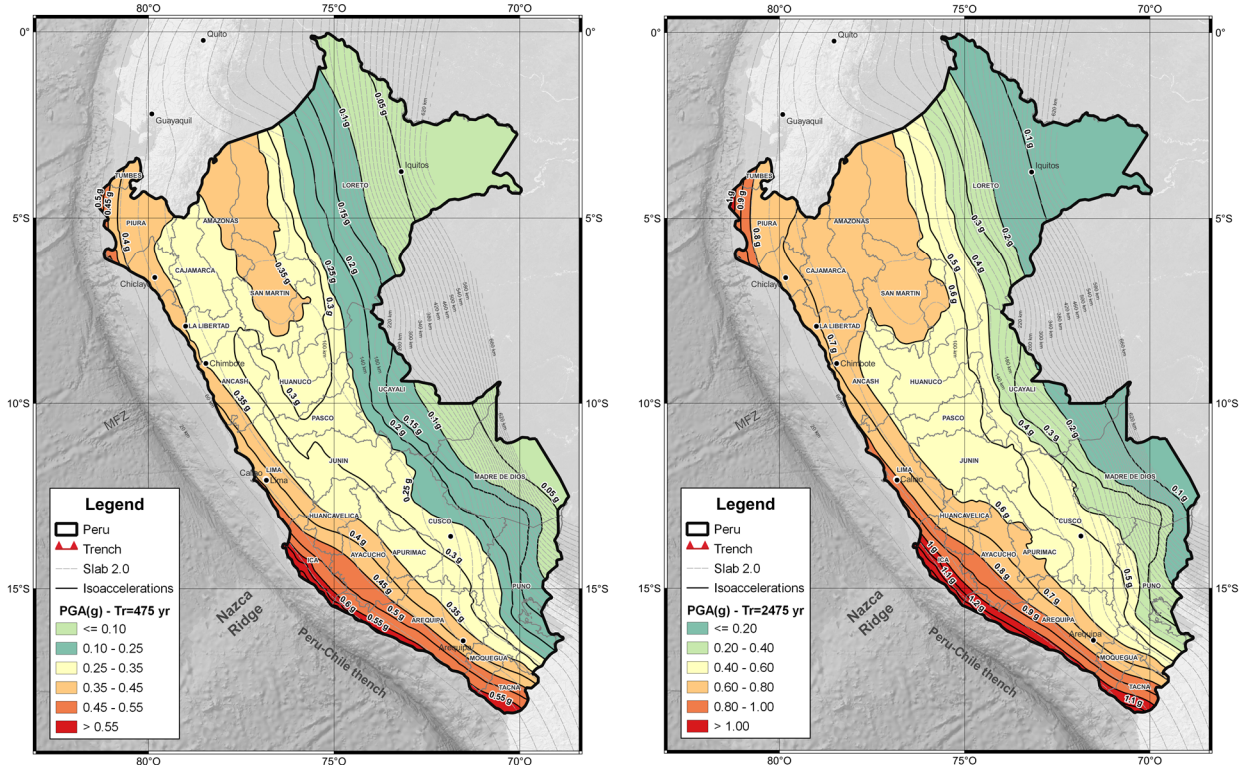


Figure 6. Seismic hazard map for 475 and 2475 year return period.

#### 4. Discussion and results

The analysis of seismic isoaccelerations in the region of Peru shows clear geographical patterns in relation to seismic hazard. It is evident that the areas close to the Peru-Chile trench and the extreme south of the country show the highest accelerations, exceeding the PGA value of 0.50 g for a Tr=475 years at some points in the departments of Ica, Arequipa and Tacna. These high accelerations are consistent with seismic hazard studies conducted in the northern Chilean region (e.g., Medina, Harmsen and Barrientos, 2017), which report values above 0.50 g in Tacna, achieving a high compatibility with the proposed Peruvian model.

On the other hand, regions more distant from the trench, such as the central and northern parts of the country, show lower accelerations, indicating a reduced seismic risk, consistent with the Ecuadorian model (e.g., Beauval *et al.*, 2018), which shows accelerations between 0.3 and 0.4 g in the area adjacent to the department of Piura and a pronounced zone with accelerations close to 0.4 g in the area adjacent to the department of Amazonas. This last zone is present in the Peruvian territory up to the department of San Martin. Likewise, the 0.3, 0.2 and 0.1 g isoacceleration curves in the zone between Ecuador and the Peruvian department of Loreto show a good correspondence.

Comparisons with hazard maps from previous studies for a Tr=475 years (Roncal, 2017; SENCICO, 2022) show that the map with acceleration lower than 0.2 g have significant differences in the northeastern region of Peru, mainly due to the inclusion of a new crustal seismotectonic source in this area. In the areas of the map with accelerations greater than 0.2 g, the values found are on average 10% higher than the acceleration values in the central and southern regions of Peru. Similarly, the greatest difference was found in the northern region, comprising the departments of San Martin and Amazonas, where the values found exceed the previously reported acceleration values by 20% and reach up to 46% at the border with Ecuador.

#### 5. Conclusions

This study has taken an integrated approach, combining traditional methods with more recent findings to provide a more accurate and up-to-date representation of seismicity in Peru, for which a seismic zonation has been performed from seismicity and geological based approaches, achieving compatibility with the interseismic moment deficit accumulation zones, rupture areas of large subduction earthquakes and maximum

magnitudes proposed by Tarazona *et al.* (2023). The proposed model consists of 34 seismic sources (7 interface, 15 intraslab and 12 crustal) with maximum magnitudes in the range of  $M_w$  8.7-9.0 for interface sources and  $M_w$  7.7-8.0 for intraslab sources.

Comparisons with seismic hazard maps from previous studies show that the results of this study are more conservative and consistent in their boundaries with studies from Chile and Ecuador (Medina, Harmsen and Barrientos, 2017; Beauval *et al.*, 2018). Therefore, the fact that the results are consistent with the interseismic moment deficit accumulation zones and rupture areas of large subduction earthquakes indicates that this approach may be a way forward for the updating of seismic hazard maps in Peru.

Finally, due to the moderate influence of crustal sources in northern Peru, a geological evaluation of the maximum magnitudes associated with the fault systems present in the Peruvian mainland is recommended for future studies.

## 6. Acknowledgments

Special thanks to ZER Geosystem Perú S.A.C and Nelson Pulido for providing the database used in this research, to Luis Sandoval, Alfredo Vargas and David's Rojas for their help with data processing.

## 7. References

- Abrahamson N., Gülerce Z. (2020). *Regionalized Ground-Motion Models for Subduction Earthquakes Based on the NGA-SUB Database (Report No. 2020/25)*. Pacific Earthquake Engineering Research Center. doi: 10.55461/SSXE9861
- Allen T., Hayes G. (2017). Alternative Rupture - Scaling Relationships for Subduction Interface and Other Offshore Environments, *Bull. Seism. Soc. of America*, 107(3): 1240-1253. doi: 10.1785/0120160255.
- ASCE (2017). *Minimum Design Loads and Associated Criteria for Buildings and Other Structures*, American Society of Civil Engineers, Virginia. doi: 10.1061/9780784414248.
- Baker J., Bradley B., Stafford P. (2021). *Seismic Hazard and Risk Analysis*. University of Cambridge Press. doi: 10.1017/9781108425056.
- Bastías N., Montalva G. (2016). Chile Strong Ground Motion Flatfile, *Earthquake Spectra*, 32(4): 2549–2566. doi: 10.1193/102715EQS158DP.
- Beauval C., Marinière J., Yepes H., Audin L., Nocquet J.M., Alvarado A., Baize S., Aguilar J., Singauch J., Jomard H. (2018). A New Seismic Hazard Model for Ecuador, *Bull. of the Seism. Soc. of America*, 108(3A): 1443–1464. doi: 10.1785/0120170259.
- Beck S., Ruff L. (1989). Great earthquakes and subduction along the Peru trench, *Physics of the Earth and Planetary Interiors*, 57(3–4): 199–224. doi: 10.1016/0031-9201(89)90112-X.
- Bommer J., Crowley H. (2017). The Purpose and Definition of the Minimum Magnitude Limit in PSHA Calculations, *Seismological Research Letters*, 88(4): 1097-1106. doi: 10.1785/0220170015.
- Cornell C. (1968). Engineering Seismic Risk Analysis, *Bulletin of the Seismological Society of America*, 58 (5): 1583–1606. doi: 10.1785/BSSA0580051583.
- Dorbath L., Cisternas A., Dorbath C. (1990). Assessment of the size of large and great historical earthquakes in Peru, *Bulletin of the Seismological Society of America*, 80(3): 551–576, doi: 10.1785/BSSA0800030551.
- Gardner J., Knopoff L. (1974). Is the sequence of earthquakes in Southern California, with aftershocks removed, Poissonian?, *Bull. of the Seism. Soc. of America*, 64(5): 1363–1367.
- Hayes G., Moore G., Portner D., Hearne M., Flamme H., Furtney M., Smoczyk G. (2018). Slab2, a Comprehensive Subduction Zone Geometry Model, *Science*, 362(6410): 58–61. doi: 10.1126/science.aat4723.
- Johnston A., Coppersmith K., Kanter L., Cornell C. (1994). *The Earthquakes of Stable Continental Regions: Assessment of Large Earthquake Potential*, Electric Power Research Institute.
- Kijko A. (2004). Estimation of the Maximum Earthquake Magnitude,  $m_{max}$ , *Pure and Applied Geophysics*, 161(8): 1655–1681, doi: 10.1007/s00024-004-2531-4.

- Kuehn N., Bozorgnia Y., Campbell K. W., Gregor N. (2020). *Partially Non-Ergodic Ground-Motion Model for Subduction Regions using the NGA-Subduction Database (Report No. 2020/04)*, Pacific Earthquake Engineering Research Center (PEER). doi: 10.55461/NZZW1930.
- Lay T. (2018). A review of the rupture characteristics of the 2011 Tohoku-oki Mw 9.1 earthquake, *Tectonophysics*, 733: 4-36. doi: 10.1016/j.tecto.2017.09.022.
- Montalva G., Bastías N., Rodriguez-Marek A. (2017). Ground-motion prediction equation for the Chilean subduction zone, *Bull. of the Seism. Soc. of America*, 107(2): 901–911. doi: 10.1785/0120160221.
- Medina F., Harmsen S., Barrientos S. (2017). “Probabilistic seismic hazard analysis for Chile”, *16th World Conference on Earthquake Engineering*, Santiago, Chile.
- National Library of Chile (2022). *Los terremotos en Chile (1570-2010)*. Available at: <https://www.memoriachilena.gob.cl/602/w3-article-3576.html> (Accessed: 24 August 2023).
- Nishenko S. (1991). Circum-Pacific Seismic Potential: 1989-1999, *Pageoph*, 135(2).
- Okal E., Borrero J., Synolakis C. (2006). Evaluation of Tsunami Risk from Regional Earthquakes at Pisco, Peru, *Bull. of the Seism. Society of America*, 96(5): 1634–1648, doi: 10.1785/0120050158.
- Ordaz M., Martinelli F., Aguilar A., Arboleda J., Meletti, C., D'Amico V. (2017). *RCRISIS. Program and platform for computing seismic hazard*.
- Pagani M., Johnson K., Garcia Palaez J. (2020). Modelling subduction sources for probabilistic seismic hazard analysis, *Geol. Society, London, Special Publications*, 501(1): 225–244, doi: 10.1144/SP501-2019-120.
- Parker G., Stewart J., Boore D., Atkinson G., Hassani B. (2020). *NGA-Subduction Global Ground-Motion Models with Regional Adjustment Factors*, Pacific Earthquake Engineering Research Center. doi: 10.55461/INKE2546.
- Pasyanos M., Masters G., Laske G., Ma Z. (2014). LITHO1.0: An Updated Crust and Lithospheric Model of the Earth, *Journal of Geophysical Research: Solid Earth*, 119(3): 2153–2173. doi: 10.1002/2013JB010626.
- Pulido N., Nakai S., Yamanaka H., Calderon D., Aguilar Z., Sekiguchi T. (2014). Estimation of a Source Model and Strong Motion Simulation for Tacna City, South Peru, *Journal of Disaster Research*, 9(6): 925–930. doi: 10.20965/jdr.2014.p0925.
- Pulido N., Aguilar Z., Tavera H., Chlieh M., Calderón D., Sekiguchi T., Nakai S., Yamazaki F. (2015). Scenario Source Models and Strong Ground Motion for Future Mega - earthquakes: Application to Lima, Central Peru, *Bulletin of the Seismological Society of America*, 105(1): 368–386. doi: 10.1785/0120140098.
- Pulido N., Villegas-Lanza J. (2023). “Mega-thrust earthquake potential along the subduction zone of Peru based on the earthquake energy-budget”, *28th General Assembly of the International Union of Geodesy and Geophysics*, Berlin, Germany. doi: 10.57757/IUGG23-3817.
- Roncal M. (2017). *Determinación del peligro sísmico en el territorio nacional y elaboración de aplicativo web*. C.E. Thesis, School of Civil Eng., Nat. Univ. of Eng., Lima, Peru.
- Scherbaum F., Delavaud E., Riggelsen C. (2009). Model Selection in Seismic Hazard Analysis: An Information-Theoretic Perspective, *Bulletin of the Seismological Society of America*, 99(6): 3234–3247. doi: 10.1785/0120080347.
- Servicio Nacional de Capacitación para la Industria de la Construcción (2016). *Actualización Del Programa de Computo Orientado a La Determinación Del Peligro Sísmico En El País*. Available at: <http://ppsh.sencico.gob.pe/static/informe.pdf> (Accessed: 11 September 2023).
- Scordilis E. (2006). Empirical Global Relations Converting Ms and mb to Moment Magnitude, *Journal of Seismology*, 10(2): 225–236, doi: 10.1007/s10950-006-9012-4.
- Silgado E. (1978). *Boletín N°3, Serie C: Geodinámica e Ingeniería Geológica: Historia de los sismos más notables ocurridos en el Perú (1513 -1974)*. Geological, Mining and Metallurgical Institute, Lima, Peru. Available at: <https://hdl.handle.net/20.500.12544/251> (Accessed: 29 August 2023).
- Sparkes, R., Tilmann, F., Hovius, N., Hillier, J. (2010). Subducted seafloor relief stops rupture in South American great earthquakes: Implications for rupture behaviour in the 2010 Maule, Chile earthquake, *Earth and Planetary Science Letters*, 298(1–2), 89–94. doi: 10.1016/j.epsl.2010.07.029.

- Stepp J. (1972). "Analysis of completeness of the earthquake sample in the Puget Sound area and its effect on statistical estimates of earthquake hazard", *Proceedings of the 1st International Conference on Microzonation*, Seattle, USA.
- Strasser F., Bommer J., Abrahamson N. (2008). Truncation of the Distribution of Ground-Motion Residuals, *Journal of Seismology*, 12(1): 79–105. doi:10.1007/s10950-007-9073-z.
- Tarazona J., Aguilar Z., Pulido N., Gonzales C., Lazares F., Miyake H. (2023). Seismicity Based Maximum Magnitude Estimation of Subduction Earthquakes in Peru, *Journal of Disaster Research*, 18(4), 308–318. doi: 10.20965/jdr.2023.p0308
- Tavera H. (2001). *Catálogo sísmico 1471-1982*, Geophysical Institute of Peru, Lima. Available at: [https://repositorio.igp.gob.pe/bitstream/handle/20.500.12816/789/cat\\_sis\\_1471\\_1982.pdf?sequence=1&isAllowed=y](https://repositorio.igp.gob.pe/bitstream/handle/20.500.12816/789/cat_sis_1471_1982.pdf?sequence=1&isAllowed=y) (Accessed: 16 September 2023).
- Tavera H., Bernal Y., Condori C., Ordaz M., Zevallos A., Ishizawa O. (2014). Re-evaluación del peligro sísmico probabilístico para el Perú, Geophysical Institute of Peru, Lima.
- Uhrhammer R. (1986). Characteristics of northern and central California seismicity, *Earthq. Notes*, 57(1): 21.
- United States Geological Survey (2020). *M 8.2 - 121 km SSE of San Pedro de Atacama, Chile. ShakeMap*. Available at: <https://earthquake.usgs.gov/earthquakes/eventpage/iscgem896170/shakemap/intensity> (Accessed: 28 September 2023).
- EPRI, U.S. DOE, U.S. NRC (2012) *Technical Report: Central and Eastern United States Seismic Source Characterization for Nuclear Facilities, Volume 1*, United States Nuclear Regulatory Commission.
- Villegas-Lanza, J., Chlieh M., Cavalié O., Tavera H., Baby P., Chire-Chira J., Nocquet J.-M. (2016). Active Tectonics of Peru: Heterogeneous Interseismic Coupling along the Nazca Megathrust, Rigid Motion of the Peruvian Sliver, and Subandean Shortening Accommodation, *Journal of Geophysical Research: Solid Earth*, 121(10): 7371–7394. doi: 10.1002/2016JB013080.
- Watts A., Koppers A., Robinson D. (2010). Seamount Subduction and Earthquakes. *Oceanography*, 23(01): 166–173. doi: 10.5670/oceanog.2010.68.
- Wheeler R. (2009). *Methods of Mmax Estimation East of the Rocky Mountains*, U.S. Geological Survey, Virginia. doi: 10.3133/ofr20091018.